REPORT 1279

THEORETICAL ANALYSIS OF INCOMPRESSIBLE FLOW THROUGH A RADIAL-INLET CENTRIFUGAL IMPELLER AT VARIOUS WEIGHT FLOWS [1]

By James J. Kramer, Vasily D. Prian, and Chung-Hua Wu

SUMMARY

A method for the solution of the incompressible nonviscous flow through a centrifugal impeller, including the inlet region, is presented. Several numerical solutions are obtained for four weight flows through an impeller at one operating speed. These solutions are refined in the leading-edge region. The results are presented in a series of figures showing streamlines and relative velocity contours. A comparison is made with the results obtained by using a rapid approximate method of analysis.

INTRODUCTION

In order to provide the fundamental information about the internal flow necessary for the rational design of efficient centrifugal compressors, two-dimensional solutions of the potential flow through centrifugal compressors on both blade-to-blade and meridional surfaces are obtained by means of relaxation methods in references 1 to 4. In addition, a three-dimensional potential-flow solution is obtained by similar means in reference 5. However, all these solutions are for impellers with inducer sections extended infinitely far upstream or to the axis of the impeller and thus yield no information concerning the flow behavior ahead of and at the entrance to blades of finite thickness or blades which are not alined with the inlet stream.

A rapid approximate method is developed in reference 6 that will predict the blade surface velocities in centrifugal impellers. The accuracy of this method is investigated therein for the region downstream of the inducer section. However, because of the lack of an exact solution of the flow in the inlet region, there has been no verification of the approximate method in that region.

Consequently, a method for analyzing the flow in a centrifugal impeller, including the inlet region, by numerical solution of the partial differential equation governing the flow was developed at the NACA Lewis laboratory and is presented herein. This method was applied to a 48-inch-diameter centrifugal impeller for both design and off-design flow conditions. The impeller is similar to that discussed in references 7 and 8. The results of the exact solution are compared with the results of the rapid approximate method of reference 6.

In addition, the flow in the region of the leading edge of the blade was determined in more detail than that obtained in the original solution. This refinement of the original solution is obtained by solving the partial differential equation in that region by relaxation methods using a grid of much finer mesh. More detailed information concerning the flow behavior near the leading edge than that obtained in the original solution is desirable, because a knowledge of the velocity gradients in this region is helpful in avoiding boundary-layer separation caused by rapidly decelerating flow. The magnitude of losses caused by boundary-layer separation at the leading edge is discussed in references 9 and 10 for sharp-nosed blades, but the manner in which the losses occur is not discussed.

ANALYSIS

The formulation of the problem and the proposed method of solution of the problem are discussed in this section.

STATEMENT OF PROBLEM

The basic assumptions which are made concerning the physical nature of the flow determine the partial differential equation governing the flow. The assigning of proper boundary conditions to the problem then determines the particular solution of the partial differential equation.

Assumptions.—The flow is assumed to be steady, incompressible, and nonviscous. The assumption of steady nonviscous flow is customary in compressor flow analyses. Several solutions have been obtained taking compressibility into account (e. g., refs. 1 and 2). The addition of the condition of compressibility complicates the solution by a factor which was considered to be out of proportion with its value in this case. Therefore, the fluid was assumed incompressible.

The further assumption is made that the flow is constrained to a blade-to-blade surface of revolution which is symmetrical about the impeller axis. Although the flow is constrained to this surface, a variation in the thickness of the stream sheet provides a closer approximation to the actual case. The shape of the stream surface in the axial-radial plane as well as the thickness variation are defined as functions of radial position, which are specified at the beginning of the solution.

[1] Supersedes NACA TN 3448, "Theoretical Analysis of Incompressible Flow Through a Radial-Inlet Centrifugal Impeller at Various Weight Flows. I—Solution by a Matrix Method and Comparison with an Approximate Method," by Vasily D. Prian, James J. Kramer, and Chung-Hua Wu, 1955; and TN 3449, "Theoretical Analysis of Incompressible Flow Through a Radial-Inlet Centrifugal Impeller at Various Weight Flows. II—Solution in Leading-Edge Region," by James J. Kramer, 1955.

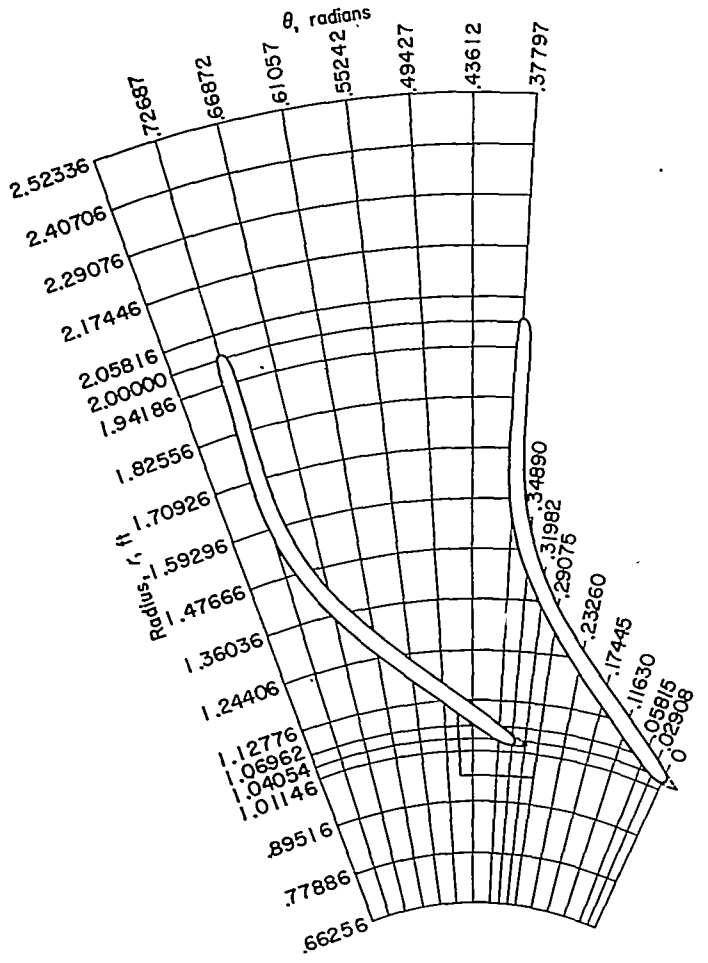

FIGURE 1.—Grid system for over-all solution.

The rear stagnation point is assumed to be located at the blade tip. The Kutta condition states that for a noncuspidate blade with a sharp trailing edge the rear stagnation point occurs at the tip. However, for an impeller with a rounded trailing edge the location of the rear stagnation point cannot be predicted. It is necessary, therefore, to assume the location of the rear stagnation point.

For the refined solution it is assumed that the values of the stream function obtained in the original solution along the boundaries of the region in which the refined solution is obtained remain unchanged during the numerical procedure of obtaining the refined solution.

Differential equation.—In this analysis, the cylindrical coordinates r, θ, and z (see figs. 1 and 2) are used. (All symbols are defined in the appendix.) The angular velocity of the impeller is denoted by ω and the fluid density by ρ. The stream-sheet thickness in the z-direction is represented by b. The trace of the stream surface in the axial-radial plane is given by specifying z as a function of r. The slope dr/dz of this curve is equal to the tangent of the angle between the axis of rotation and the tangent to the trace of the stream surface in the axial-radial plane and is denoted by λ (see fig. 2). Thus, the resultant velocity w is given by

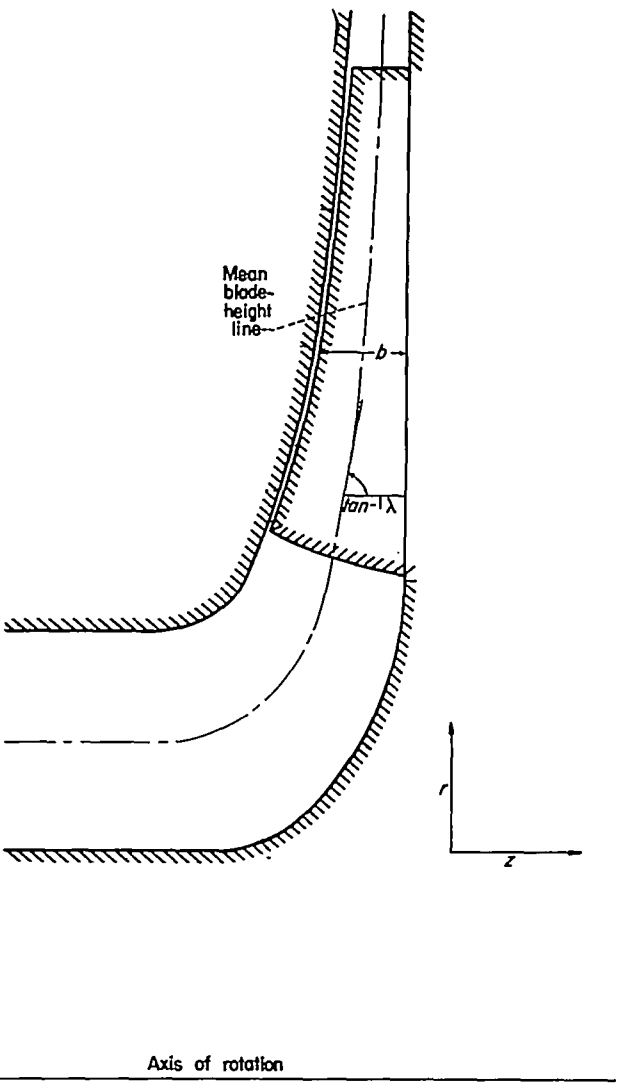

FIGURE 2.—Axial-radial plane view of 48-inch-diameter centrifugal impeller.

$$w^2=w_\theta^2+w_r^2\left(1+\frac{1}{\lambda^2}\right)$$

where the subscripts r and θ indicate components in the r- and θ-directions, respectively.

The stream function Ψ is defined by the following differential equations:

$$\frac{\partial\Psi}{\partial r}=-b\rho w_\theta \tag{1a}$$

$$\frac{\partial\Psi}{\partial\theta}=rb\rho w_r \tag{1b}$$

In this report all derivatives with respect to r shall be understood to mean derivatives with respect to r on the stream surface; that is, $\partial/\partial r$ in this report shall correspond to the bold-faced $\partial/\partial r$ of reference 11, in which the differential equation for the type flow considered herein is derived. With these

definitions and assumptions, the differential equation of the flow becomes (see ref. 11, p. 35)

$$\frac{\partial^2\Psi}{\partial r^2}+\left(\frac{1}{r}-\frac{\partial \ln b}{\partial r}\right)\frac{\partial\Psi}{\partial r}+\frac{1}{r^2}\left(1+\frac{1}{\lambda^2}\right)\frac{\partial^2\Psi}{\partial\theta^2}=2\omega b\rho \qquad (2)$$

This equation, together with the boundary conditions, mathematically determines the problem.

Boundary conditions.—This analysis of the flow is a boundary-value problem of the first kind or a Dirichlet problem. Certain boundaries of the flow and the values of the stream function on these boundaries are specified. Furthermore, the flow is assumed to vary periodically in the circumferential direction, completing a cycle in one pitch angle, the angular distance between two adjacent blade mean lines. The rotational speed of the impeller and the weight flow through the compressor are also specified. The domain of the solution is extended sufficiently far upstream and downstream so that the flow is assumed to be uniform at the upstream and downstream boundaries. With the addition of these conditions, the problem is determined mathematically.

For the refined solution the boundary conditions are obtained from the original solution. The value of the stream function, expressed as a dimensionless ratio of the weight flow through a single passage, on the blade surface is equal to 1; the values along the other boundaries are obtained from cross plots of the original data. The error involved in reading values from the cross plots was less than 0.0003 with values of Ψ/M ranging from 0 to 1.

METHOD OF OBTAINING SOLUTION FOR FLOW THROUGH ENTIRE BLADE PASSAGE

Superposition of four basic solutions.—The differential equation (eq. (2)) was solved by a superposition of four basic solutions. These four basic solutions form a set of linearly independent solutions such that all possible flows (including all tip speeds) are expressible as linear combinations of these basic solutions. The first of these, designated ψ_0, is a solution of equation (2) with the condition that no flow crosses the upstream and downstream boundaries and $\omega=\omega_0\neq 0$.

The other three basic solutions, designated ψ_1, ψ_2, and ψ_3, are solutions of the linear homogeneous equation obtained by equating the left side of equation (2) to zero. Thus, if

$$L=\frac{\partial^2}{\partial r^2}+\left(\frac{1}{r}-\frac{\partial \ln b}{\partial r}\right)\frac{\partial}{\partial r}+\frac{1}{r^2}\left(1+\frac{1}{\lambda^2}\right)\frac{\partial^2}{\partial\theta^2}$$

then ψ_1, ψ_2, and ψ_3 are solutions of

$$L(\psi)=0$$

Because L is a linear operator, ψ_0 plus linear combinations of ψ_1, ψ_2, and ψ_3 will satisfy equation (2) for $\omega=\omega_0$.

Boundary conditions for four basic solutions.—The flow region is represented by abcdefgh in sketch (a):

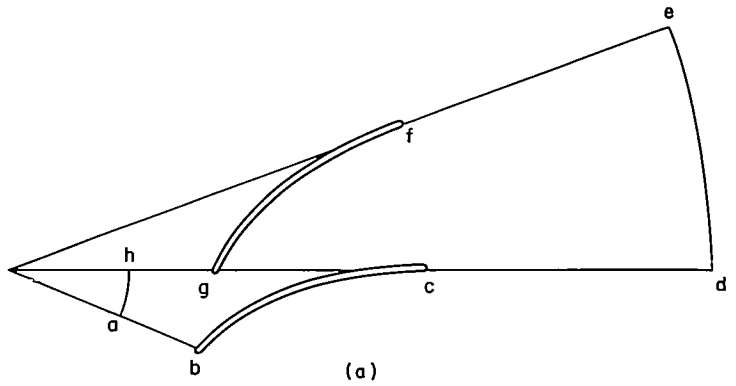

The upstream and downstream boundaries, ah and de, respectively, are placed sufficiently far from the blades so that flow conditions can be assumed uniform at these stations. The angular distance from a to h and from d to e is one pitch angle. For all the basic solutions, the condition that the flow is periodic about the axis of rotation with a period of one pitch angle makes it possible to obtain the solutions without a knowledge of the stream function along ab and gh. The finite-difference equation for points along these lines is obtained in the same manner as in reference 12. For the solution ψ_0 in which the flow is that induced only by the rotation of the impeller without any through flow, the value of ψ along ah and de is specified zero, indicating no flow crossing the upstream and downstream boundaries. The values along the blade surfaces bc and gf are also specified as zero. The solution to equation (2) for these boundary conditions is designated ψ_0.

The through-flow solution, that is, the flow through the stationary blade row, is obtained from linear combinations of three basic solutions to the homogeneous equation obtained by equating the left side of equation (2) to zero. All possible flows through the stationary blade row can be represented by linear combinations of these basic solutions. It can be seen from the boundary conditions shown in the following table that these three basic solutions are linearly independent:

Basic solution	Boundary values at point—			
	a	d	e	h
ψ_0	0	0	0	0
ψ_1	0	0	1	1
ψ_2	−1	0	1	0
ψ_3	−1	−1	0	0

The value of ψ along the trailing face is specified as zero and along the driving face as 1 for all three solutions. That these independent solutions are sufficient for the construction of all possible through flows can be seen from the following consideration.

Any flow is determined when the upstream and downstream flow conditions are specified. The velocity is assumed to be constant at stations ah and de. Hence, the stream function varies linearly from a to h and from d to e. Since the angular distance from a to h and from d to e is one pitch angle and the flow is assumed to vary periodically about the axis with a period of one pitch angle, the specification of conditions at points a, d, and h fixes the solution. The value of ψ is constant along both the driving and trailing faces, with the difference between the function values being equal to $\psi_h-\psi_a$. The choice of 0 and ± 1 as the values of ψ at points a, h, d, and e and along bc and gf represents no restriction since these three basic solutions remain solutions to the homogeneous equation when changed by a multiplicative or additive constant.

Coefficients of ψ_0, ψ_1, ψ_2, and ψ_3 in linear combinations.—The final solution Ψ for any weight flow or rotational speed will be obtained from an equation of the form

$$\Psi=A_0\psi_0+A_1\psi_1+A_2\psi_2+A_3\psi_3 \tag{3}$$

The coefficients A_0, A_1, A_2, and A_3 are determined by the specification of four independent physical conditions: (1) the rotational speed, (2) the weight flow, (3) the location of the rear stagnation point, and (4) the irrotationality of the absolute flow.

The coefficient A_0 is determined by the rotational speed and is given by

$$A_0=\frac{\omega}{\omega_0} \tag{4}$$

That is, A_0 is the ratio of the rotational speed ω for the desired solution to that used in obtaining the basic solution ω_0.

The change in Ψ across one blade passage is equal to the weight flow through a single passage. Therefore,

$$A_1+A_2+A_3=M \tag{5}$$

where M is the weight flow through a single passage.

The rear stagnation point is assumed to be at the blade tip. Thus, at the tip

$$w_{\theta,t}=0$$

or

$$\left(\frac{\partial\Psi}{\partial r}\right)_t=0 \tag{6}$$

This derivative is expressed in finite-difference form for the grid point at the blade tip and with equation (3) yields a linear relation in A_0, A_1, A_2, and A_3.

The absolute flow is irrotational; therefore, if r_1 and r_2 are radial stations upstream of the blade row, the following equation holds:

$$\int_0^{2\pi}(w_{\theta,2}+\omega r_2)r_2\,d\theta-\int_0^{2\pi}(w_{\theta,1}+\omega r_1)r_1\,d\theta=0 \tag{7}$$

where the subscripts 1 and 2 indicate values along the lines $r=r_1$ and $r=r_2$, respectively. If r_1 is chosen equal to the value of r at the upstream boundary, equation (7) becomes

$$\int_0^{2\pi} r_2 w_{\theta,2}\,d\theta=-2\omega\pi r_2^2 \tag{8}$$

since $w_{\theta,1}$ is equal to $-\omega r_1$. When the stream-function definition (eq. (1a)) is introduced, equation (8) becomes

$$\int_0^{2\pi}\frac{\partial\Psi}{\partial r}\,d\theta=2\pi\omega\rho b_2 r_2 \tag{9}$$

Equation (9) can be integrated numerically to yield a linear relation in A_0, A_1, A_2, and A_3.

Equations (4) to (6) and (9) form a system of four independent simultaneous linear equations in four unknowns, A_0, A_1, A_2, and A_3.

Numerical method of obtaining basic solutions.—The region of solution was covered with a network of grid lines whose intersections form grid or nodal points, as shown in figure 1.

The solution for a given set of boundary conditions of the differential equation was obtained at each of these grid points by solving the set of linear simultaneous equations obtained when the differential equation is written in finite-difference form for each grid point. A five-point system was used in the finite-difference approximation of the derivatives. This procedure is equivalent to approximating the stream function by a fourth-degree polynomial in the neighborhood of the grid point. The solution of the set of n linear simultaneous equations was obtained on high-speed digital computers by the matrix method outlined in reference 12. Since there were four basic solutions, four sets of n simultaneous linear equations were solved by this process.

METHOD OF OBTAINING REFINED SOLUTION IN LEADING-EDGE REGION

Relaxation method.—The solution of equation (2) was obtained by means of relaxation techniques (ref. 13) in the region outlined by the bold lines in figure 1. The residuals of the relaxation process were reduced to a value indicating unit change in the fifth decimal place of the stream function. This degree of accuracy is consistent with the accuracy of the cross plots used to obtain the boundary values.

Grid.—The grid used in the relaxation process is shown in figure 3. The density of the grid lines is greatest in the region of the leading edge and decreases gradually in both directions. This type of grid assured greatest accuracy in the region of main interest. The ratio of the grid spacing in either direction at a point is never greater than 2.5 and usually less than or equal to 2.0. The intersections of the grid lines are called grid points. The grid points in the interior of the boundaries are the points at which the numerical solution is obtained. There were 138 interior grid points for this problem.

Finite-difference approximation.—The derivatives of equation (2) were written in finite-difference form with a three-point system used. In the original solution a five-point

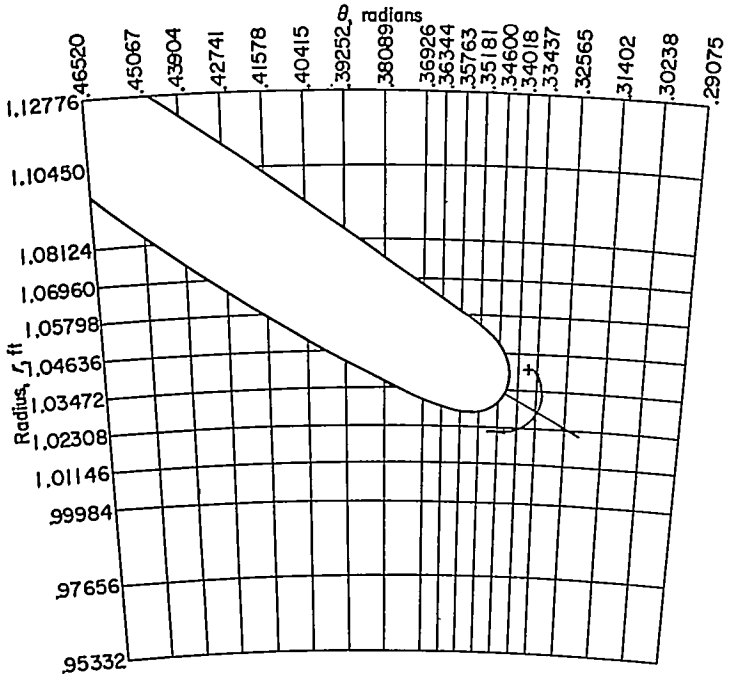

FIGURE 3.—Grid system for refined solution.

system was used. Because of the fineness of the grid, a three-point system was considered adequate for this problem.

NUMERICAL EXAMPLE

The previously outlined methods were applied in order to analyze the flow in a 48-inch-diameter radial-inlet centrifugal impeller. A description of the geometry of the impeller and the operating conditions for which the analysis was carried out follow.

Geometry of impeller.—The impeller investigated was a 48-inch-tip-diameter radial-inlet centrifugal impeller having 18 blades, similar to the one discussed in references 7 and 8. The sharp leading edge and blunt trailing edge were rounded as shown in figure 1 because of practical computing considerations. The blade coordinates are given in table I. The solution was obtained on the surface generated by rotating the mean blade-height line about the axis of rotation. This line was approximated by the following function:

$$z=\frac{-0.041456}{(r-0.40828)}+\text{constant} \tag{10}$$

The streamline spacing in the axial-radial plane is not known. Therefore, the stream-sheet thickness b in the z-direction was approximated by the blade height in the z-direction. This parameter was approximated by the following function:

$$b=0.07208+1.01517e^{-1.54601r} \tag{11}$$

The parameter λ is equal to dr/dz of the stream-surface trace in the axial-radial plane and from equation (10) is given by

$$\frac{1}{\lambda}=\frac{0.041456}{(r-0.40828)^2} \tag{12}$$

Operating conditions.—Four solutions were obtained corresponding to four weight flows at a tip speed of 700 feet per second. These four weight flows, which are the same as those of reference 7, are shown in the following table:

Case	Weight flow, M, lb/sec
A	14.00
B	26.25
C	32.10
D	44.00

RESULTS AND DISCUSSION

The results of the solutions obtained by the application of the previously outlined methods are presented in figures 4 to 11, which show streamlines and constant relative velocity contours. The over-all solution for the entire blade passage as obtained by the matrix method is shown in the (a) part of each figure and the refined solution for the leading-edge region in the (b) part. Figures 4 to 11 are projections on the $r\theta$-plane; that is, the curvature of the stream surface in the axial-radial plane is neglected. The comparison with the results of the approximate method described in reference 6 is made in figure 12.

STREAMLINES

The distribution of stream function is shown by means of contours of constant stream-function ratio Ψ/M in figures 4 to 7 for the four weight flows investigated. The impeller tip speed was 700 feet per second for all four cases.

Case A.—In figure 4 the streamlines for a weight flow of 14 pounds per second are shown. This condition is the incipient surge weight flow for the experimental case (ref. 7). A large eddy attached to the driving face of the blade extends from $r\sim1.31$ to $r\sim1.84$ and almost one-third the distance across the passage between blades at its widest point. The major part of the flow is concentrated in the region near the trailing face, while the eddy and other relatively low-momentum fluid occupy half the channel.

The inlet stagnation point occurs on the driving face of the blade at $r\sim1.05$, and the local angle of attack is 80°. The local angle of attack is defined as the angle between the tangents to the blade mean line and the stagnation streamline. The sign convention for angle of attack, shown in figure 3, is chosen so that flow directed at the driving face results in a positive angle of attack. The slip factor, the ratio of the mass-averaged absolute tangential velocity of the fluid at the tip to the absolute tip speed, is equal to 0.874.

Case B.—The streamline pattern for a weight flow of 26.25 pounds per second is shown in figure 5. This weight flow is sufficiently high to eliminate the eddy on the driving face of the blade. However, a fairly large concentration of low-momentum air is still present, so that halfway through the impeller 50 percent of the fluid occupies more than two-thirds the available flow area. The slip factor at the impeller tip is 0.873, and the local angle of attack is approximately 6°.

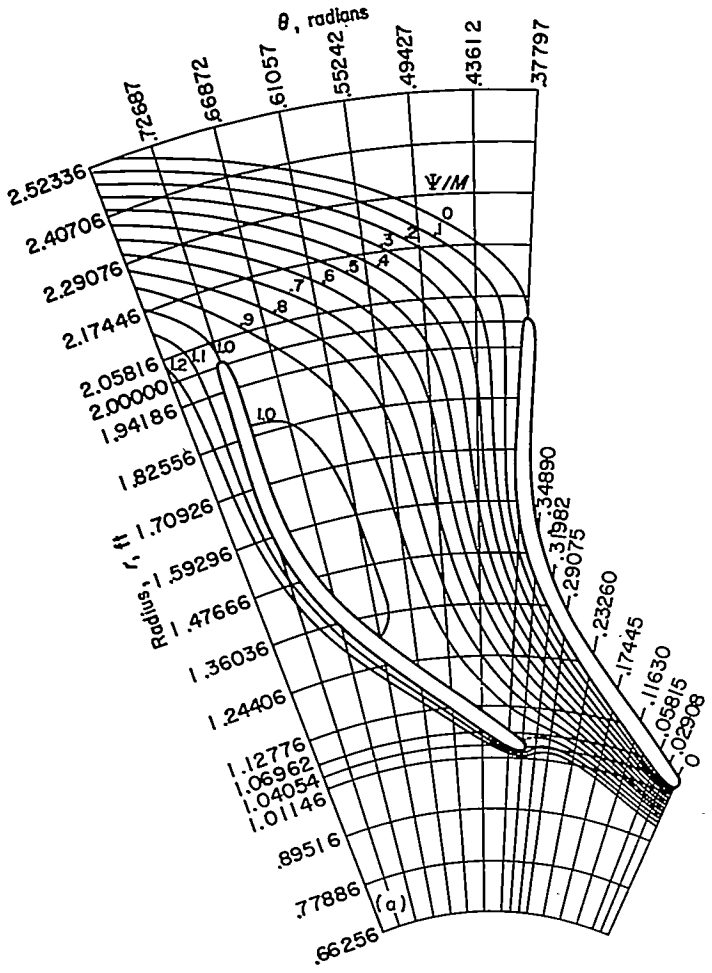

(a) Entire blade passage.

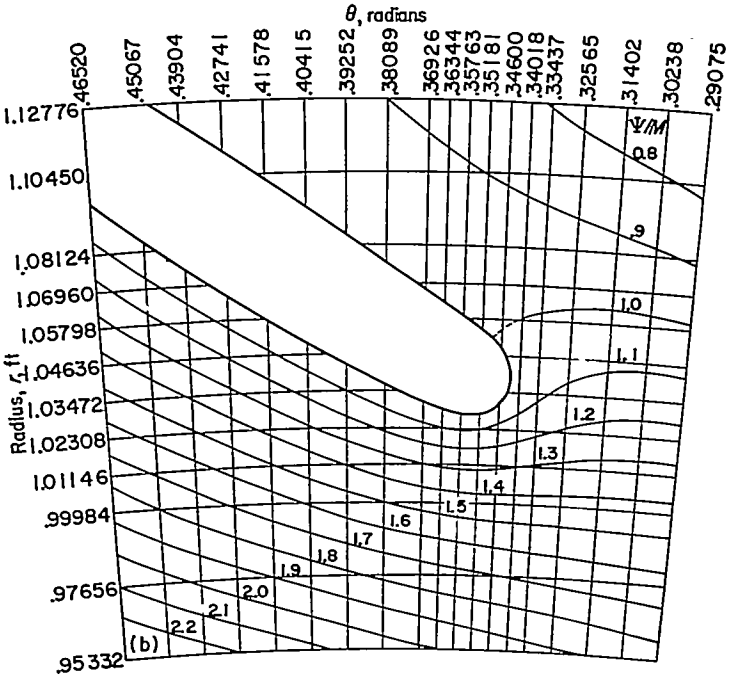

(b) Leading-edge region.

FIGURE 4.—Streamlines for weight flow of 14 pounds per second (case A).

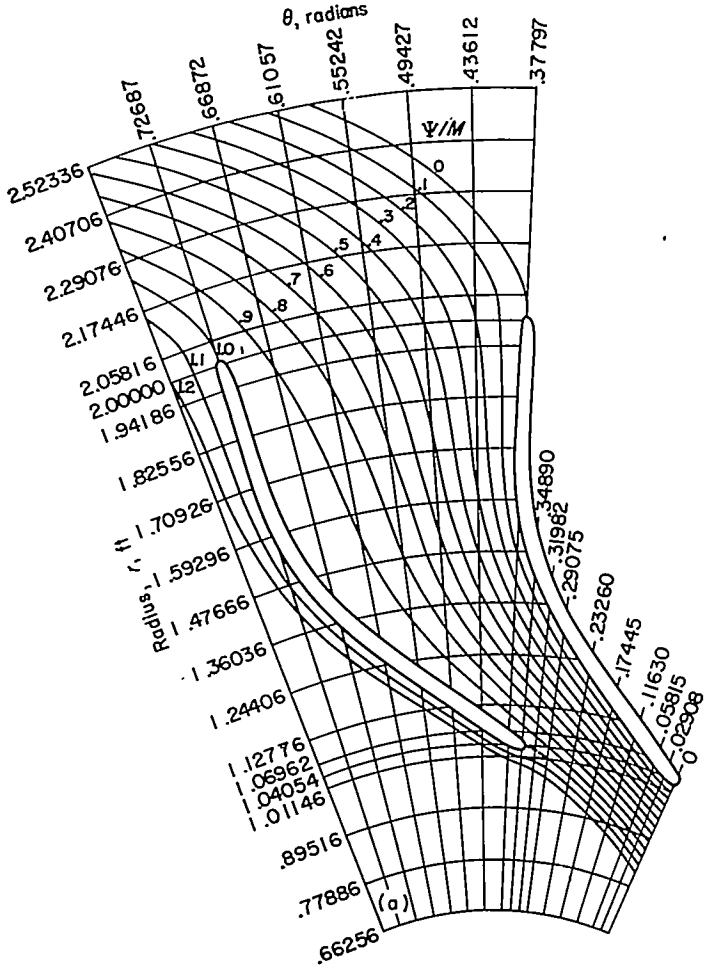

(a) Entire blade passage.

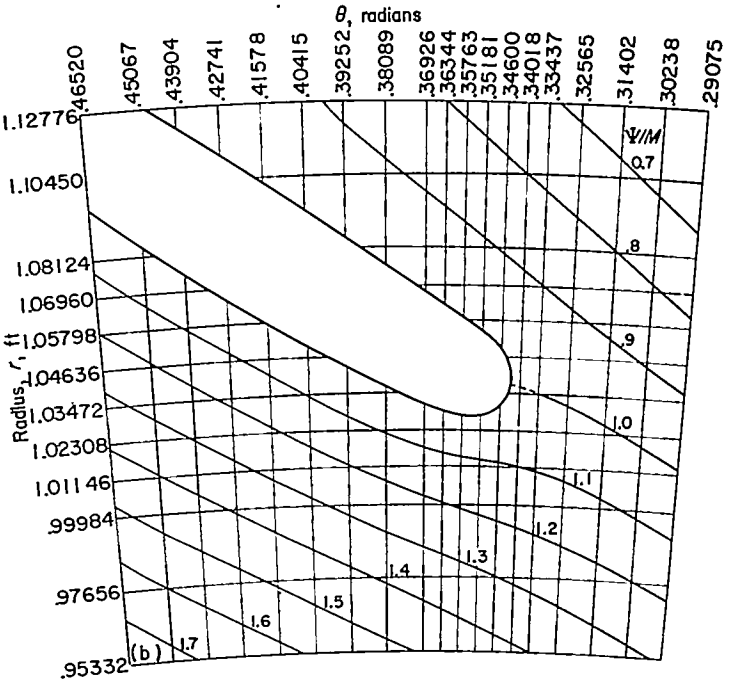

(b) Leading-edge region.

FIGURE 5.—Streamlines for weight flow of 26.25 pounds per second (case B).

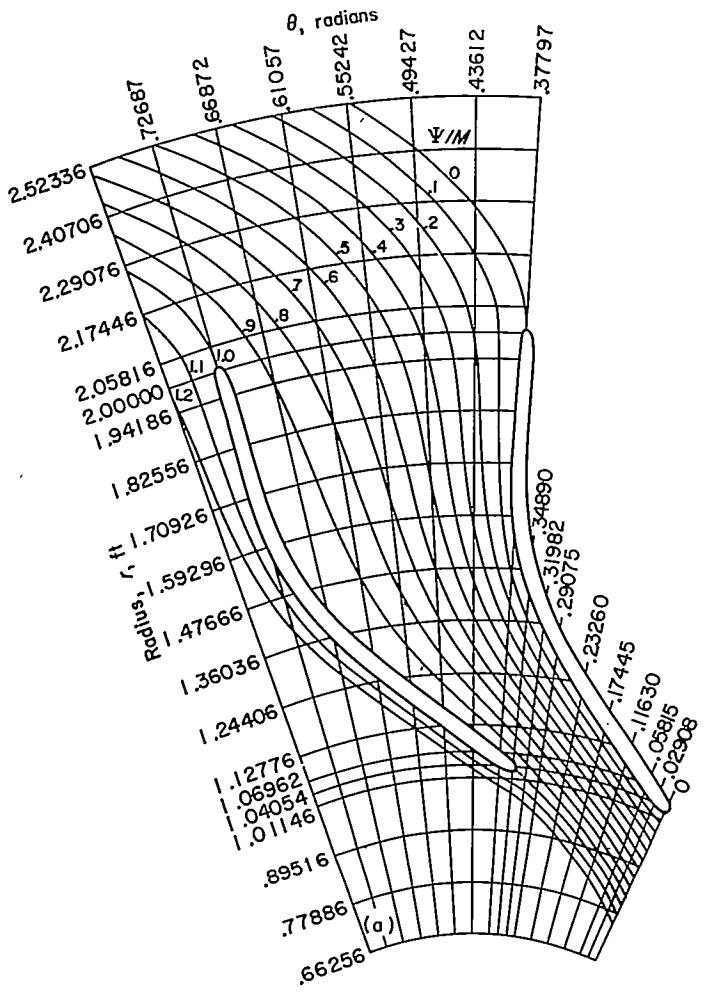

(a) Entire blade passage.

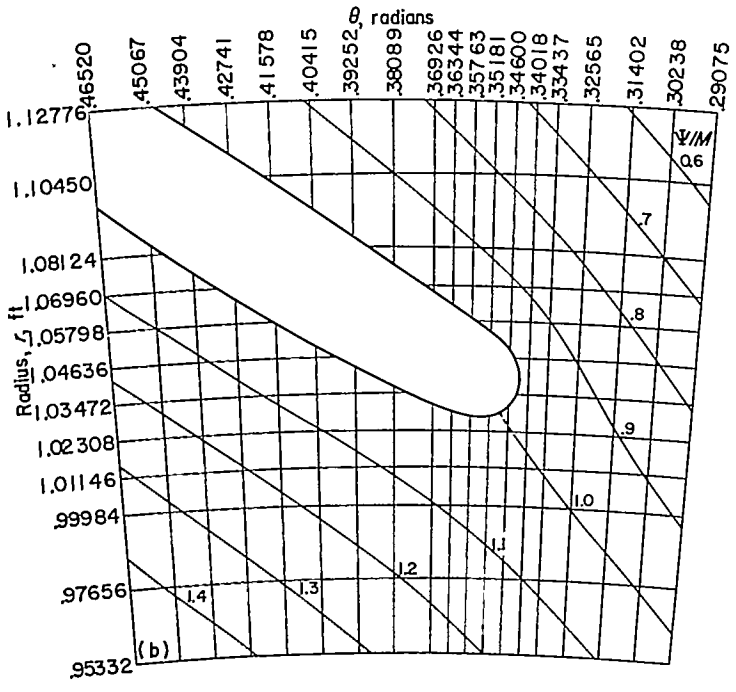

(b) Leading-edge region.

FIGURE 6.—Streamlines for weight flow of 32.10 pounds per second (case C).

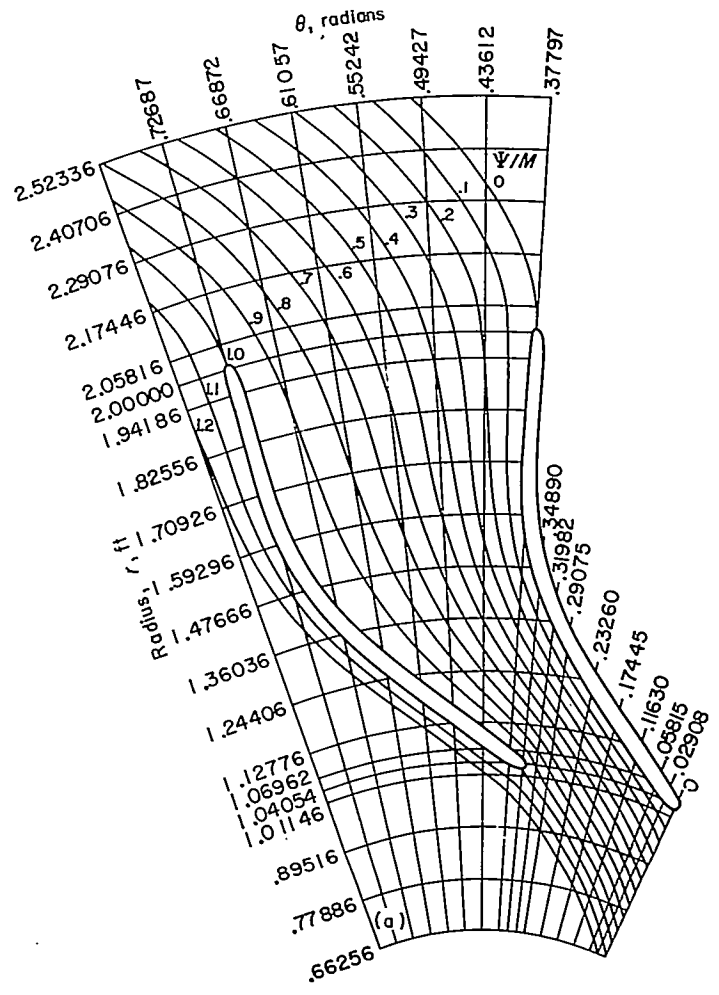

(a) Entire blade passage.

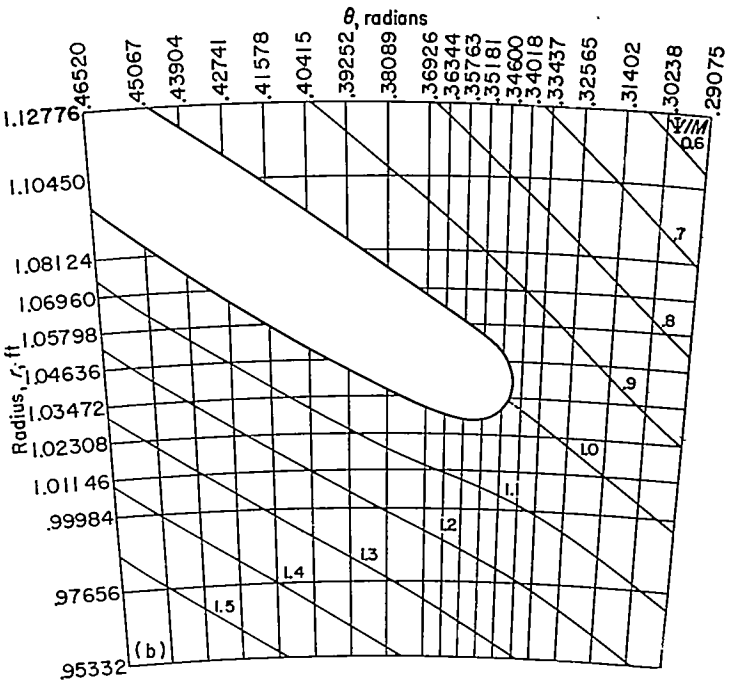

(b) Leading-edge region.

FIGURE 7.—Streamlines for weight flow of 44 pounds per second (case D).

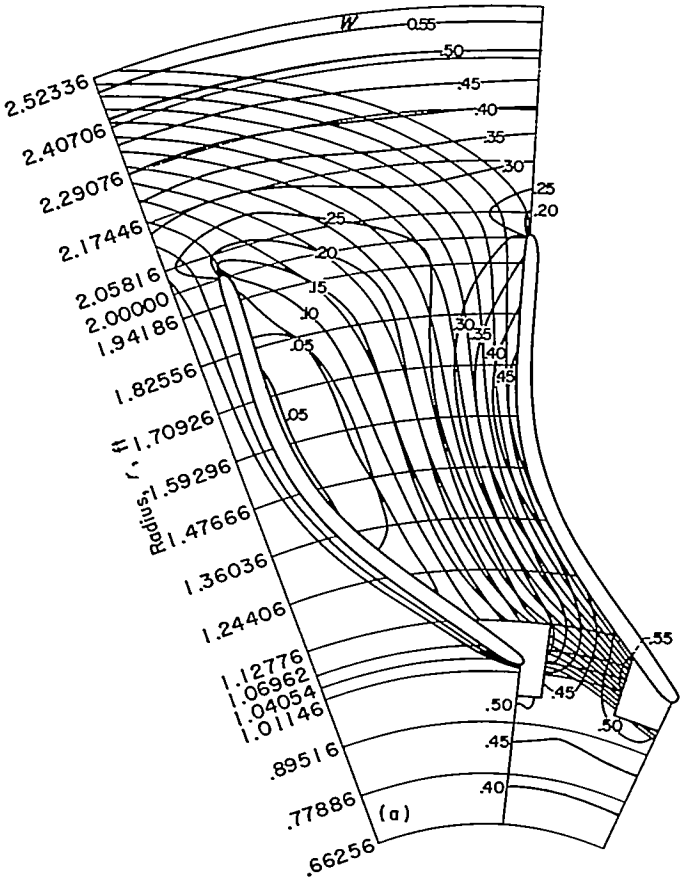

(a) Entire blade passage.

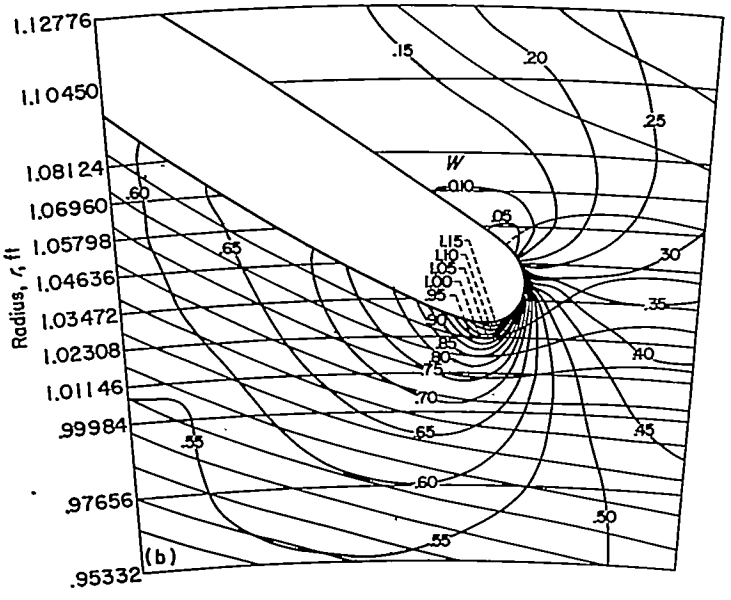

(b) Leading-edge region.

FIGURE 8.—Contours of constant relative velocity ratio W for weight flow of 14 pounds per second (case A).

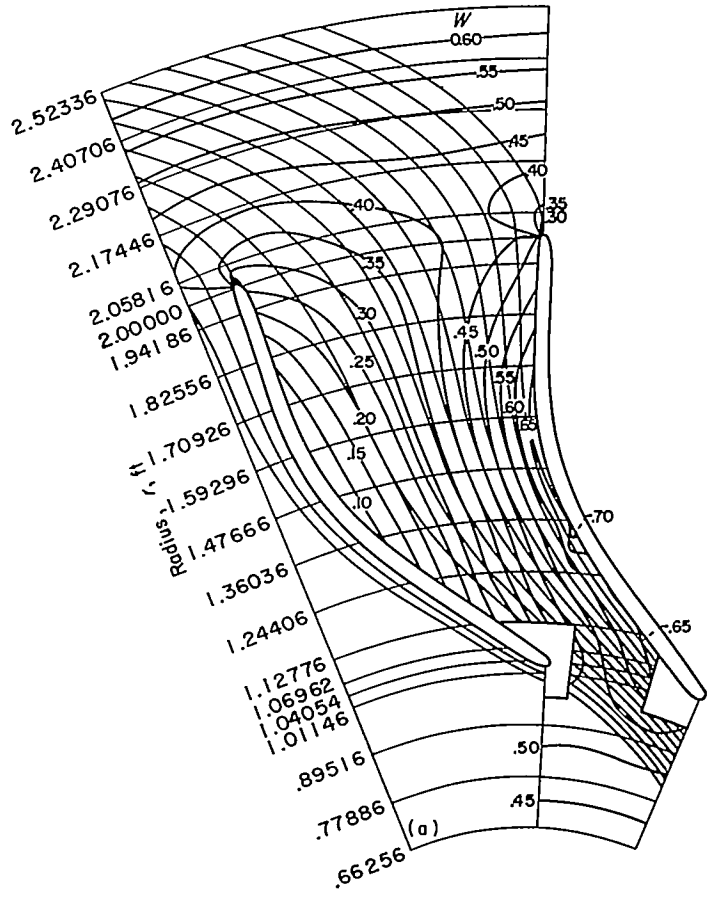

(a) Entire blade passage.

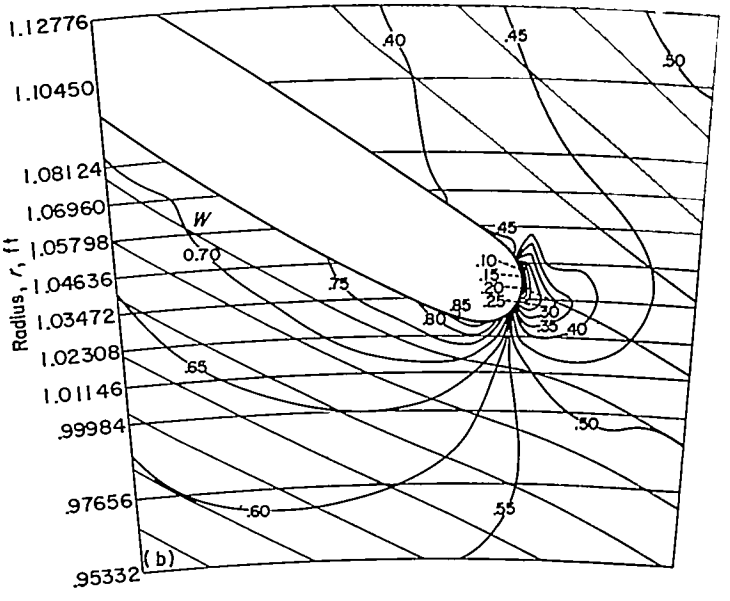

(b) Leading-edge region.

FIGURE 9.—Contours of constant relative velocity ratio W for weight flow of 26.25 pounds per second (case B).

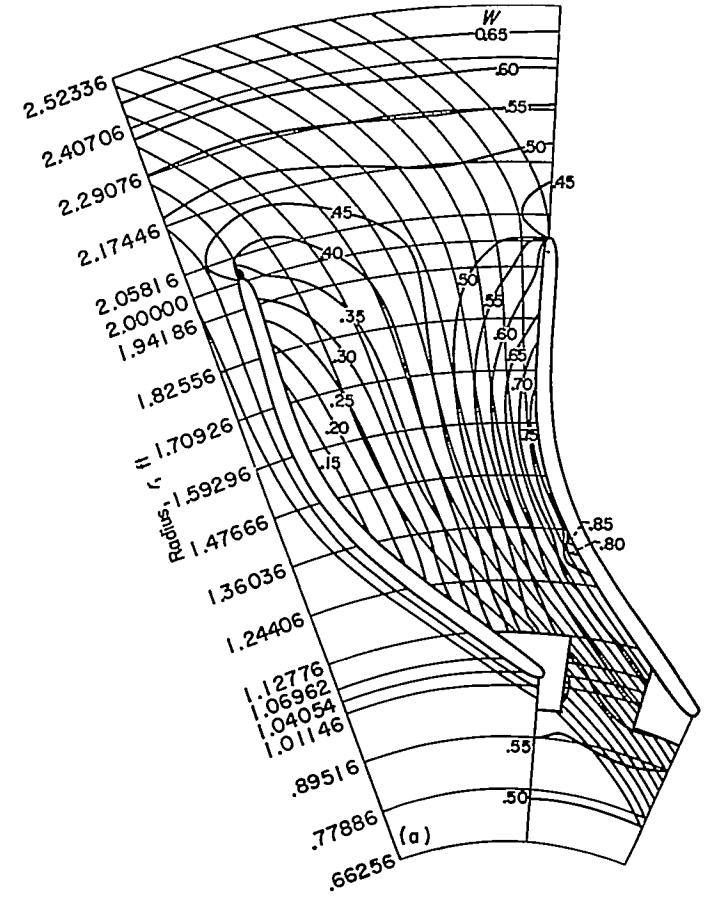

(a) Entire blade passage.

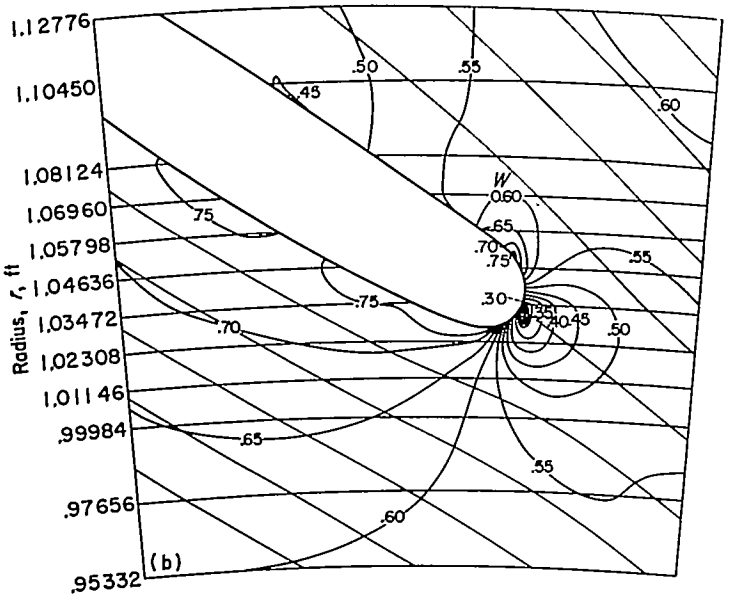

(b) Leading-edge region.

FIGURE 10.—Contours of constant relative velocity ratio W for weight flow of 32.10 pounds per second (case C).

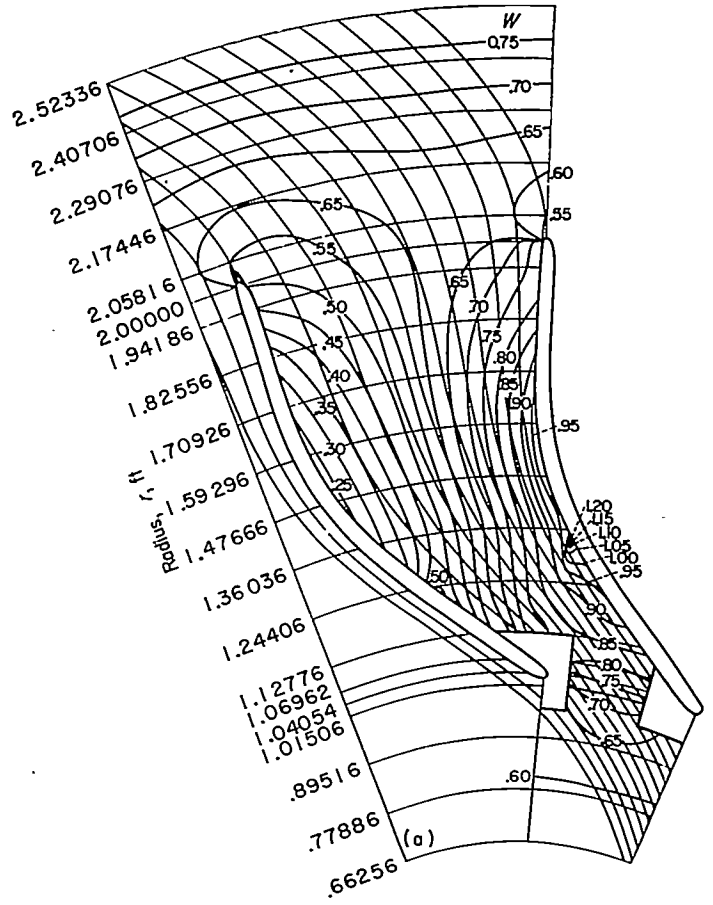

(a) Entire blade passage.

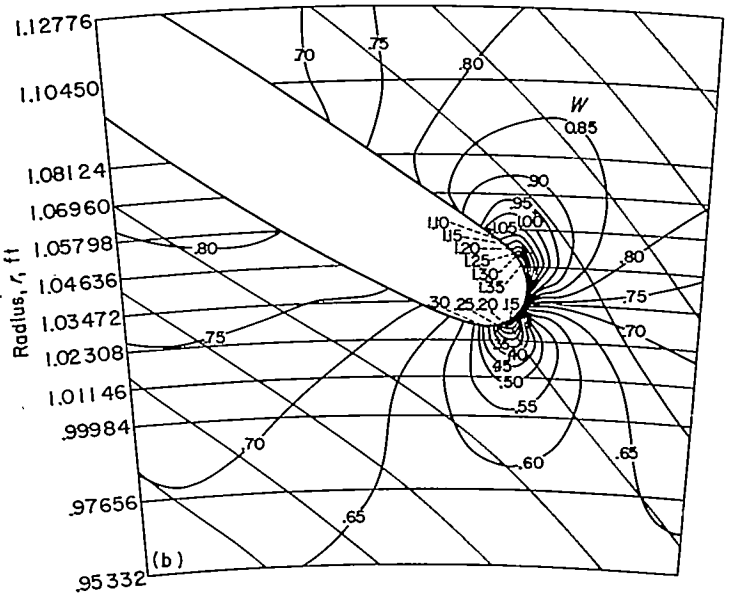

(b) Leading-edge region.

FIGURE 11.—Contours of constant relative velocity ratio W for weight flow of 44 pounds per second (case D).

Case C.—The streamline pattern for a weight flow of 32.10 pounds per second (fig. 6) is similar to that for 26.25 pounds per second because of the comparatively small change in weight flow. However, the local angle of attack changes considerably, from 6° for case B to −7° for case C. This sensitivity of local angle of attack to weight flow changes is quite marked over the entire weight flow range investigated. The weight flow for zero local angle of attack is about 29 pounds per second.

The flow continues to shift toward the driving face, and the slip factor at the tip is 0.871.

Case D.—In figure 7, the streamline pattern is shown for a weight flow of 44 pounds per second. In the investigation reported in reference 7, this represented the maximum weight flow. The flow is distributed across the passage more nearly uniformly than in the other examples. The flow ceases to be perfectly guided at $r \sim 1.5$, as occurred for all other weight flows. The slip factor at the tip for this condition is 0.859, so that the total variation in slip factor from surge to maximum weight flow as determined in reference 7 is 0.015. The inlet stagnation point occurs on the trailing face at $r \sim 1.028$. Thus, the stagnation point shifts about 0.022 foot as the weight flow increases from 14 to 44 pounds per second. The local angle of attack for case D is −28° so that the total range of local angle of attack investigated was from 80° to −28°.

RELATIVE VELOCITY

Contours of constant relative velocity ratio W (relative velocity divided by tip speed) are shown in figures 8 to 11. In the figures showing the entire blade-passage ((a) parts), the velocities near the leading edge are not shown. Reference should be made to the figures showing the leading-edge region only ((b) parts).

Case A.—For a weight flow of 14 pounds per second (fig. 8) a stagnation point occurs where the eddy begins to form at $r \sim 1.31$ on the driving face. Velocities are low along the entire driving face with slightly negative velocities in the eddy region. A rapid acceleration followed by a less rapid deceleration occurs on the leading edge and the trailing face because of the large positive local angle of attack.

Case B.—In figure 9 the velocity contours for a weight flow of 26.25 pounds per second are shown. Downstream of the leading-edge region the velocity along the trailing face is nearly constant (except for a small acceleration and deceleration at $r \sim 1.3$ to $r \sim 1.7$). In the leading-edge region, small local decelerations occur on both the driving and trailing faces with the one on the trailing face being the larger. Flow conditions in the leading-edge region are better for this weight flow than for any of the other weight flows investigated.

Case C.—The velocity contours for a weight flow of 32.10 pounds per second are presented in figure 10. At $r \sim 1.3$ on the trailing face, a slight acceleration occurs followed by a rapid deceleration. This velocity peak is caused by the beginning of more rapid blade curvature at that point.

For case C a larger deceleration occurs on the driving face than for case B. Decelerations are probably more serious on the driving face than on the trailing face because the low-momentum air caused by the deceleration aggravates the secondary-flow conditions. These secondary flows transport the low-momentum fluid on the driving face to the trailing face. This type of motion is discussed in more detail in reference 14.

It was previously noted that the weight flow for zero local angle of attack is about 29 pounds per second. However, zero local angle of attack is not necessarily desirable for rounded leading edges such as the one considered herein. In view of the velocity contours of the 26.25- and 32.10-pound-per-second cases, a slight positive local angle of attack seems desirable. For a weight flow of 29 pounds per second, a greater deceleration would probably occur on the driving face than that which occurs for a weight flow of 26.25 pounds per second. This appears to be the case since the leading edge is shaped so that at zero local angle of attack the flow on the blade surfaces would be roughly symmetrical about the blade mean line. Consequently, it seems advisable to design the leading-edge regions in the manner suggested in reference 15 and further discussed in reference 16. These leading-edge contours are characterized by very little curvature of the driving face so that flow alined with the driving face would produce little or no local deceleration.

Case D.—The velocity contours for a weight flow of 44 pounds per second are plotted in figure 11. The flow along the driving and trailing faces is similar to that for case C, because in both cases the inlet flow is directed toward the trailing face. The local acceleration and deceleration on the trailing face at $r \sim 1.3$ is more pronounced for this case.

A very large deceleration occurs on the driving face just downstream of the leading edge. This deceleration is about the same size as that which occurred on the trailing face in case A. The deceleration is probably more serious on the driving face because of its contribution to the buildup of secondary flows. Also, at sufficiently high weight flows the separation following a rapid deceleration will induce choking before the theoretical maximum weight flow is attained.

MEAN ANGLE OF ATTACK

The approximate mean angle of attack, that is, the angle between the mean flow direction at the inlet and the tangent to the blade mean line, was computed from the rotational speed and the average inlet velocity. The average inlet velocity was computed from the weight flow and the annular area. Two values were used for the annular area: (1) the total annular area with no blade blockage assumed, and (2) the total annular area minus the blockage caused by the blades. The thickness of the blades used in the latter computation was that at the 1.04-foot radius, which was approximately the radius at which maximum blade thickness in the tangential direction occurred. The mean angle of attack across the passage at the 1.04-foot radius was also computed from the exact solution. These are compared in the following table:

Weight flow, M, lb/sec	Mean angle of attack, deg, based on—		
	Unblocked annulus	Blocked annulus	Exact solution
14.00	12.3	9.2	0
26.25	.1	−4.6	−5.3
32.10	−4.9	−10.0	−9.0
44.00	−13.6	−19.0	−15.4

The sign convention for the angle of attack is such that a positive angle of attack indicates flow directed toward the driving face of the blade. From the comparison of these angles of attack, it is apparent that the mean angle of attack is best predicted by basing the calculations on the annular area with blade blockage considered. The poor agreement between the mean angle of attack of the exact solution and that based on the blocked-inlet annular area at the lowest weight flow is probably caused by the eddy. It appears that inlet flow alined with the driving face results in good flow conditions in the leading-edge region. The blade angle of the driving face just downstream of the rounded leading edge is 57°, whereas the angle between the mean line and the radial direction is 62°. Thus, for case B the average inlet flow angle would approximately equal the driving-face blade angle. Flow conditions in the leading-edge region for case B seemed to be the best of the conditions investigated.

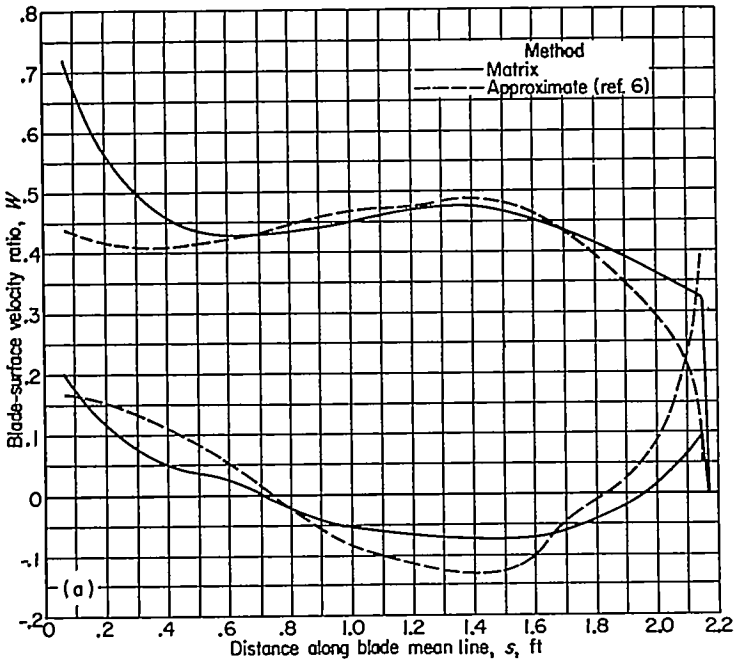

(a) Weight flow, 14 pounds per second (case A).

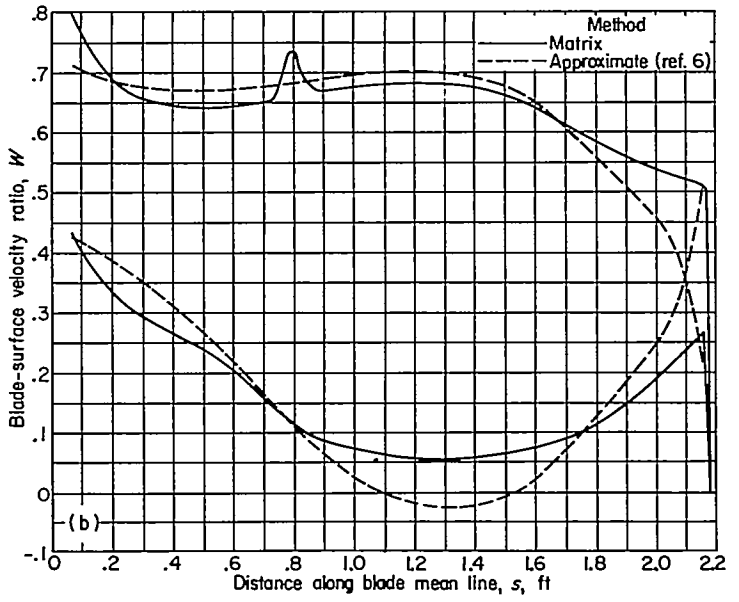

(b) Weight flow, 26.25 pounds per second (case B).

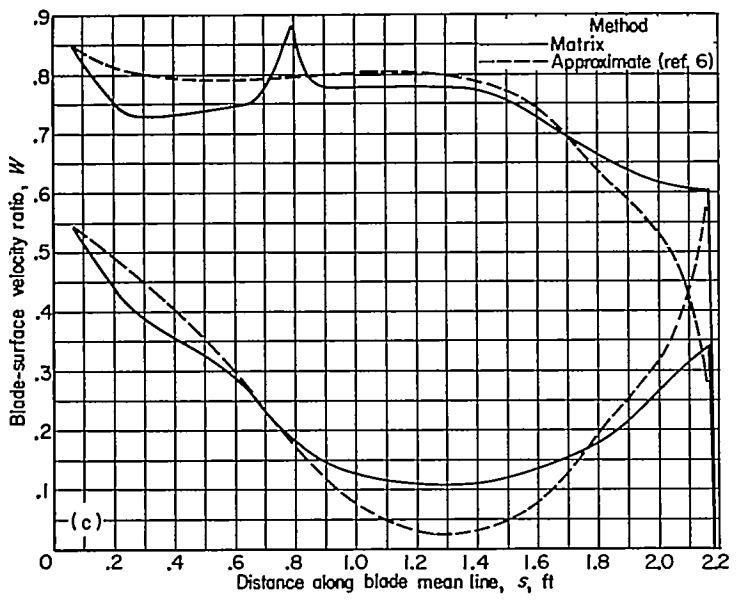

(c) Weight flow, 32.10 pounds per second (case C).

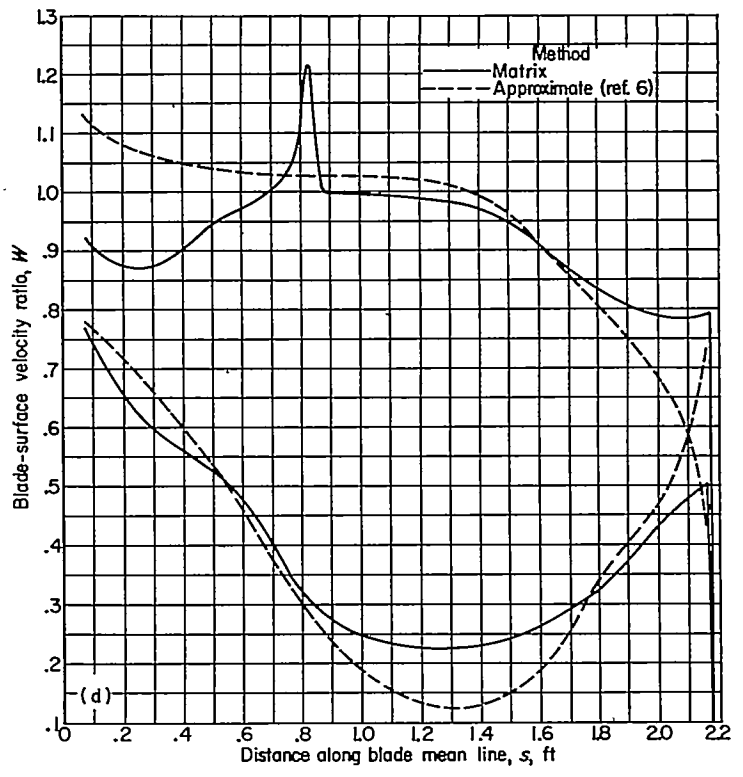

(d) Weight flow, 44 pounds per second (case D).

FIGURE 12.—Comparison of blade-surface velocity ratios obtained by approximate and matrix methods.

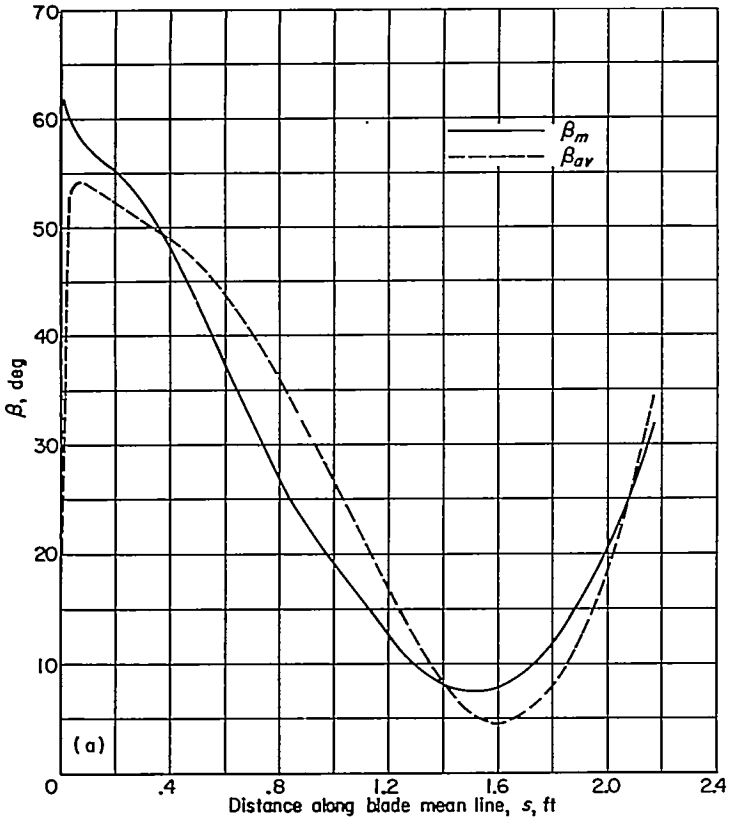

(a) Weight flow, 14 pounds per second (case A).

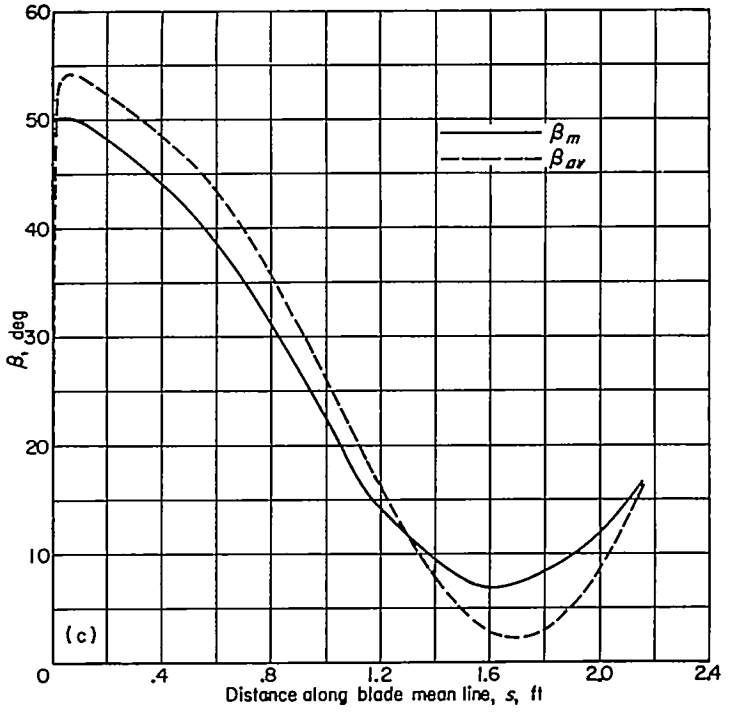

(c) Weight flow, 32.10 pounds per second (case C).

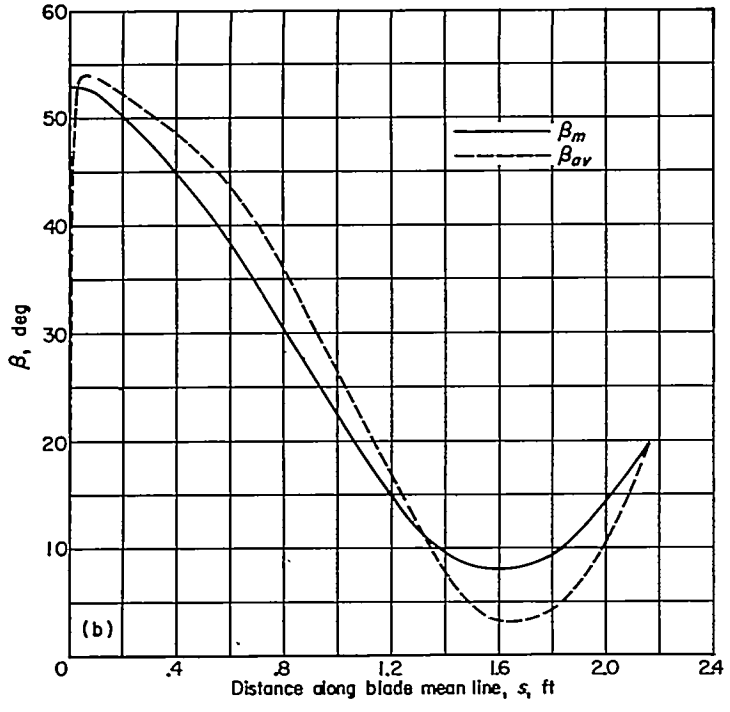

(b) Weight flow, 26.25 pounds per second (case B).

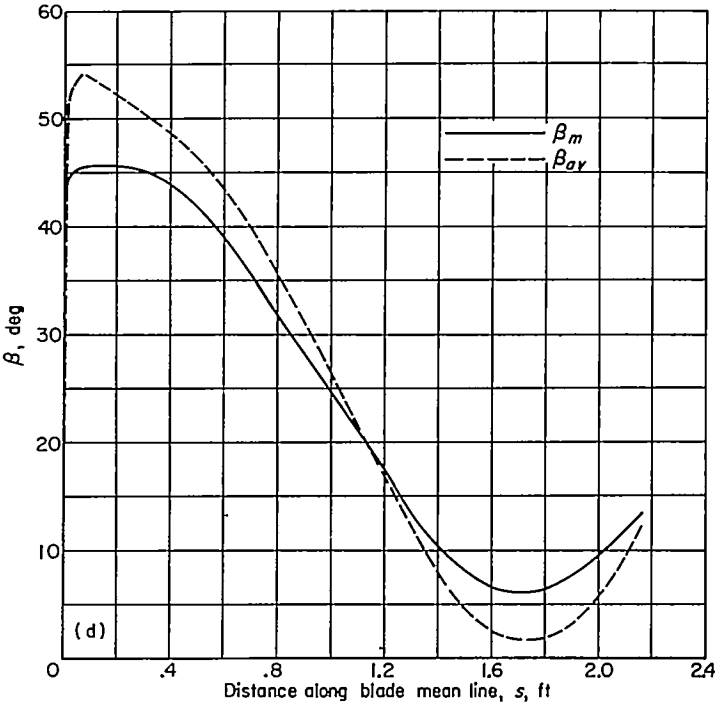

(d) Weight flow, 44 pounds per second (case D).

FIGURE 13.—Comparison of mass-averaged flow angle of exact solution β_m with approximation of β_m used in approximate method β_{av}.

COMPARISON WITH APPROXIMATE METHOD

The blade surface velocities for the four weight flows were computed by the rapid approximate method of reference 6 in order to determine the accuracy of the approximate method, especially in the inlet region, by comparison with the matrix solution. In figure 12, the surface velocity ratios as computed by the approximate method are compared with the surface velocity ratios as determined by the matrix method. The velocity ratios are plotted against distance s along the blade mean line.

In the approximate method the "average" values of W and β are values which satisfy the one-dimensional continuity equation. The "average" velocity ratio is assumed equal to the average of the blade surface velocity ratios W_{av}. The "average" flow angle is assumed equal to β_{av}, the average of the blade surface angles, for values of $s \leq 1.34$. For $s > 1.34$, the "average" flow angle is approximated by a parabolic variation (with r) between the average of the blade surface angles at $s=1.34$ and the flow angle at the tip as determined by the slip factor. The slope $d\beta_{av}/dr$ at $s=1.34$ is used as the third condition to determine the parabola. The approximate flow angle as given by the parabolic variation is also denoted by β_{av}. It is difficult to evaluate these assumptions separately. In order to get some idea of their validity, the mass-averaged flow angle β_m is compared with β_{av} in figure 13, and the mass-averaged velocity ratio W_m is compared with W_{av} in figure 14.

It was impossible to obtain meaningful results in the region of the rounded leading edge. This failure of the approximate method is caused by the invalidity of the assumption that β_m is equal to β_{av}. For values of s such that $0.07 \leq s \leq 0.6$, the surface velocities are predicted adequately for cases B and C but poorly for cases A and D. For case A the failure

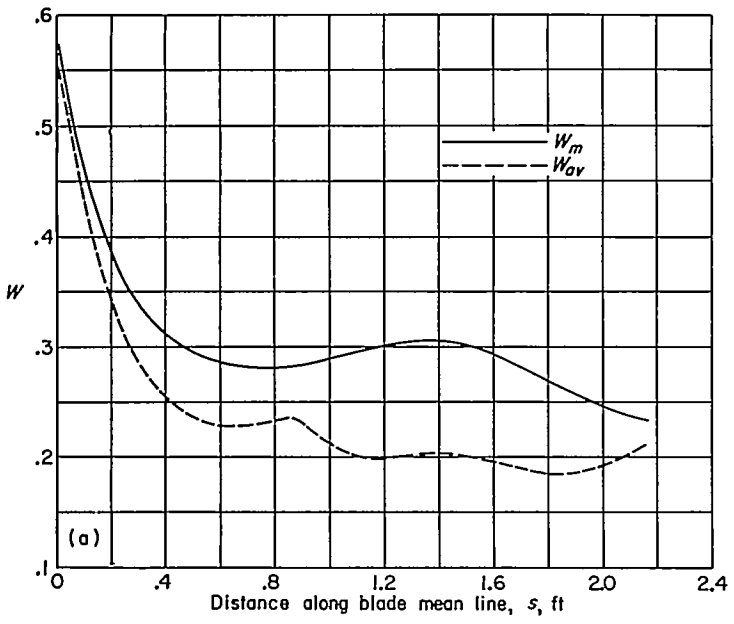

(a) Weight flow, 14 pounds per second (case A).

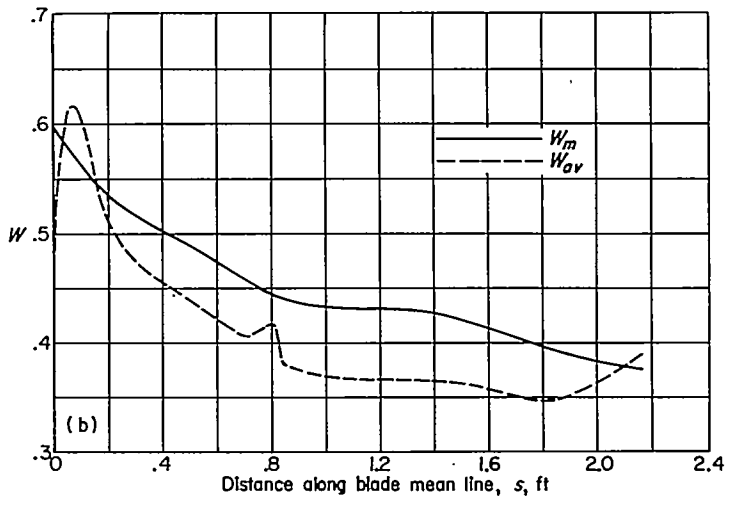

(b) Weight flow, 26.25 pounds per second (case B).

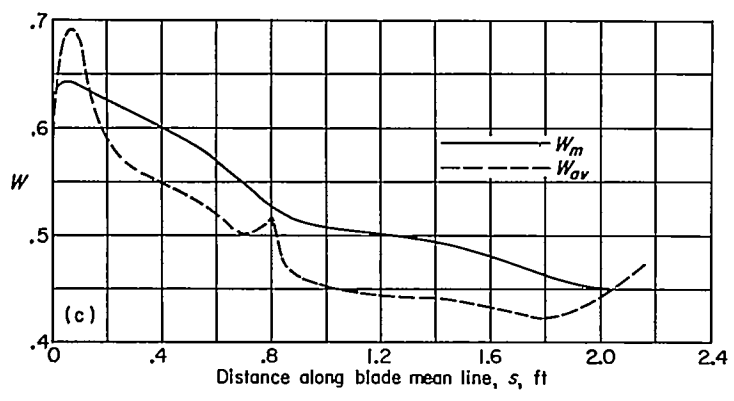

(c) Weight flow, 32.10 pounds per second (case C).

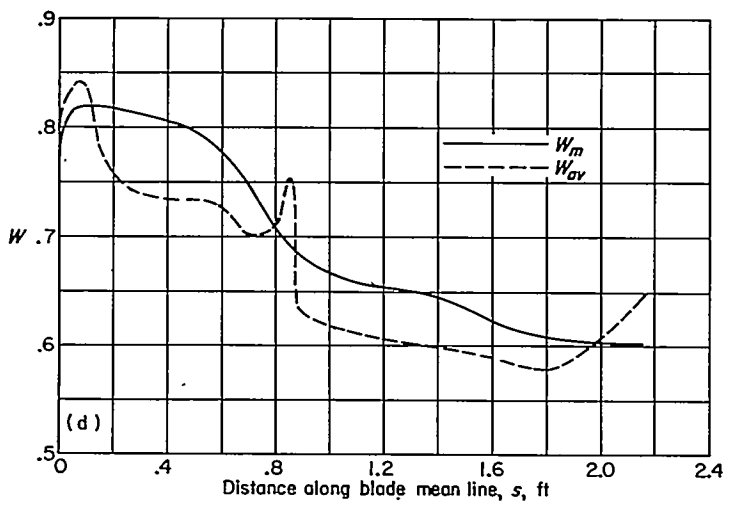

(d) Weight flow, 44 pounds per second (case D).

FIGURE 14.—Comparison of mass-averaged relative velocity ratio W_m with average of blade-surface velocity ratios W_{av}.

is probably caused by the change in the relative size of β_{av} and β_m. At $s=0.6$, β_{av} is greater than β_m but then becomes less than β_m as s decreases. This trend is not followed in the other cases. For case D the agreement of W_{av} with W_m and of β_{av} with β_m is poorer for $s<0.6$ than for the other cases. The trends for case D, however, were the same as for cases B and C.

In the region $0.6\leq s\leq 1.8$, the agreement between the approximate solution and the exact solution is adequate (except in the neighborhood of $s=0.8$ for cases B, C, and D) for approximately predicting both the velocity and the velocity gradients for all four weight flows. Such good agreement is surprising for case A, because the agreement between W_m and W_{av} and between β_m and β_{av} is not nearly so good for case A as it is for the other cases; the eddy attached to the driving face for case A is the cause of this poor agreement.

For $s>1.8$, the agreement between the approximate method and the exact method is poor, and β_{av} is less than β_m for all four cases except near the tip in case A. This reverse in trend, together with the fact that the blade surface angles differ by a large amount, probably is the reason for the failure of the approximate method near the tip. In the region $s>1.34$, β_{av} is determined by a parabolic approximation to β_m. Since β_{av} and β_m agree fairly well at $s=1.34$ and at the tip, the failure of the parabolic approximation must be attributed to incorrect values of $d\beta_{av}/dr$ at $s=1.34$ or to the inadequacy of a parabolic approximation.

SUMMARY OF RESULTS

A method for the solution of the incompressible nonviscous flow through a centrifugal impeller (including the inlet region) is presented and is applied to a 48-inch-diameter centrifugal impeller. Solutions for the entire blade passage were obtained for four weight flows ranging from incipient surge to maximum as determined by actual impeller tests. In addition, these solutions were refined in the leading-edge region. The blade surface velocities obtained by the matrix solutions for the entire blade passage were compared with those obtained by a rapid approximate method of analysis. The following results were noted:

1. A large eddy formed on the driving face of the blade at the incipient surge weight flow but was not present for the three higher weight flows.
2. The slip factor varied from 0.874 to 0.859 as the weight flow increased.
3. For weight flows of 26.25, 32.10, and 44 pounds per second, a local acceleration followed by a rapid deceleration occurred on the trailing face of the blades at a radius of about 1.3 feet, that is, where the blade begins to curve more rapidly.
4. The stagnation point shifted from the driving to the trailing face of the blade as the weight flow increased, while the local angle of attack varied from 80° to −28°.
5. A small positive local angle of attack seems desirable for rounded leading-edge blades.
6. Of the four weight flows investigated, flow conditions around the blade nose were the best for the weight flow corresponding to an angle of attack of −4.6° computed from blade speed and an upstream radial-axial velocity for which blade blockage had been taken into account.
7. The rapid approximate method was adequate in the inlet region just downstream of the leading edge for weight flows of 26.25 and 32.10 pounds per second. These weight flows corresponded to mean angles of attack of −5.3° and −9.0°, respectively.
8. The mean angle of attack was best predicted by basing the approximate computation on the weight flow, the tip speed, and the annular area minus the blockage of the blades.

Lewis Flight Propulsion Laboratory
National Advisory Committee for Aeronautics
Cleveland, Ohio, *March 4, 1955*

APPENDIX

SYMBOLS

The following symbols are used in this report:

A_0, A_1, A_2, A_3	coefficients in eq. (3)
b	stream-sheet thickness in z-direction, ft
M	weight flow through single passage, lb/sec
r	radial distance, ft
s	distance along blade mean line, ft
W	ratio of relative velocity to tip speed
w	relative velocity, ft/sec
z	axial distance, ft
β	flow angle, deg
θ	angular coordinate in relative system, radians
λ	slope of trace of stream surface in axial-radial plane
ρ	fluid density, lb/cu ft
Ψ	stream function, eqs. (1)
ψ_0,ψ_1, ψ_2,ψ_3	basic solutions
ω	angular velocity of impeller, radians/sec

Subscripts:

av	approximation to averaged value used in approximate method
m	mass-averaged value
r	component in radial direction
t	impeller tip
θ	component in tangential direction
0	value in basic solution of eq. (2)
1,2	conditions along $r=r_1$ and $r=r_2$, respectively

REFERENCES

1. Stanitz, John D., and Ellis, Gaylord O.: Two-Dimensional Compressible Flow in Centrifugal Compressors with Straight Blades. NACA Rep. 954, 1950. (Supersedes NACA TN 1932.)
2. Ellis, Gaylord O., and Stanitz, John D.: Two-Dimensional Compressible Flow in Centrifugal Compressors with Logarithmic-Spiral Blades. NACA TN 2255, 1951.
3. Ellis, Gaylord O., Stanitz, John D., and Sheldrake, Leonard J.: Two Axial-Symmetry Solutions for Incompressible Flow Through a Centrifugal Compressor with and without Inducer Vanes. NACA TN 2464, 1951.
4. Stanitz, John D., and Ellis, Gaylord O.: Two-Dimensional Flow on General Surfaces of Revolution in Turbomachines. NACA TN 2654, 1952.
5. Ellis, Gaylord O., and Stanitz, John D.: Comparison of Two- and Three-Dimensional Potential-Flow Solutions in a Rotating Impeller Passage. NACA TN 2806, 1952.
6. Stanitz, John D., and Prian, Vasily D.: A Rapid Approximate Method for Determining Velocity Distribution on Impeller Blades of Centrifugal Compressors. NACA TN 2421, 1951.
7. Michel, Donald J., Ginsburg, Ambrose, and Mizisin, John: Experimental Investigation of Flow in the Rotating Passages of a 48-Inch Impeller at Low Tip Speeds. NACA RM E51D20, 1951.
8. Prian, Vasily D., and Michel, Donald J.: An Analysis of Flow in Rotating Passage of Large Radial-Inlet Centrifugal Compressor at Tip Speed of 700 Feet Per Second. NACA TN 2584, 1951.
9. Kramer, James J., and Stanitz, John D.: Prediction of Losses Induced by Angle of Attack in Cascades of Sharp-Nosed Blades for Incompressible and Subsonic Compressible Flow. NACA TN 3149, 1955.
10. Wright, Linwood C.: Approximate Effect of Leading-Edge Thickness, Incidence Angle, and Inlet Mach Number on Inlet Losses for High-Solidity Cascades of Low Cambered Blades. NACA TN 3327, 1954.
11. Wu, Chung-Hua: A General Theory of Three-Dimensional Flow in Subsonic and Supersonic Turbomachines of Axial-, Radial-, and Mixed-Flow Types. NACA TN 2604, 1952.
12. Wu, Chung-Hua, and Brown, Curtis A.: A Theory of the Direct and Inverse Problems of Compressible Flow Past Cascade of Arbitrary Airfoils. Jour. Aero. Sci., vol. 19, no. 3, Mar. 1952, pp. 183–196.
13. Southwell, R. V.: Relaxation Methods in Theoretical Physics. Clarendon Press (Oxford), 1946.
14. Hamrick, Joseph T., Mizisin, John, and Michel, Donald J.: Study of Three-Dimensional Internal Flow Distribution Based on Measurements in a 48-Inch Radial-Inlet Centrifugal Impeller. NACA TN 3101, 1954.
15. Weinig, F.: Die Strömung um die Schaufeln von Turbomaschinen. Johann Ambrosius Barth (Leipzig), 1935.
16. Stanitz, John D.: Effect of Blade-Thickness Taper on Axial-Velocity Distribution at the Leading Edge of an Entrance Rotor-Blade Row with Axial Inlet, and the Influence of This Distribution on Alinement of the Rotor Blade for Zero Angle of Attack. NACA TN 2986, 1953.

435875—57——43

TABLE I.—MODIFIED BLADE COORDINATES

Driving face		Trailing face	
r, ft	θ, radians	r, ft	θ, radians
1. 0405	0. 34256	1. 0285	0. 34890
1. 0521	. 34890	1. 0352	. 37797
1. 0696	. 37224	1. 0405	. 38604
1. 0740	. 37797	1. 0518	. 40705
1. 1190	. 43612	1. 0696	. 43273
1. 1278	. 44633	1. 0971	. 46520
1. 1711	. 49427	1. 1278	. 49939
1. 2324	. 55242	1. 1511	. 52335
1. 2441	. 56242	1. 2144	. 58150
1. 3095	. 61057	1. 2441	. 60413
1. 3604	. 63995	1. 2974	. 63965
1. 4262	. 66872	1. 3525	. 66872
1. 4767	. 68476	1. 3604	. 67227
1. 5930	. 70726	1. 4283	. 69780
1. 7093	. 71497	1. 4767	. 71113
1. 8256	. 71601	1. 5600	. 72687
1. 9419	. 71601	1. 5930	. 73041
2. 0000	. 72080	1. 7093	. 73583
2. 0123	. 72687	1. 8256	. 73416
		1. 9419	. 73312
		2. 0000	. 73145
		2. 0123	. 72687